

A snapback-free TOL-RC-LIGBT with vertical P-collector and N-buffer design

Weizhong Chen(陈伟中), Yao Huang(黄垚), Lijun He(贺利军), Zhengsheng Han(韩郑生), Yi Huang(黄义)

Citation: Chin. Phys. B . 2018, 27(8): 088501. **doi:** 10.1088/1674-1056/27/8/088501

Journal homepage: http://cpb.iphy.ac.cn; http://iopscience.iop.org/cpb

What follows is a list of articles you may be interested in

Closed-form breakdown voltage/specific on-resistance model using charge superposition technique for vertical power double-diffused metal-oxide-semiconductor device with high-κ insulator

Xue Chen(陈雪), Zhi-Gang Wang(汪志刚), Xi Wang(王喜), James B Kuo
Chin. Phys. B . 2018, 27(4): 048502. **doi:** 10.1088/1674-1056/27/4/048502

Ultra-low specific on-resistance high-voltage vertical double diffusion metal-oxide-semiconductor field-effect transistor with continuous electron accumulation layer

Da Ma(马达), Xiao-Rong Luo(罗小蓉), Jie Wei(魏杰), Qiao Tan(谭桥), Kun Zhou(周坤), Jun-Feng Wu(吴俊峰)
Chin. Phys. B . 2016, 25(4): 048502. **doi:** 10.1088/1674-1056/25/4/048502

One-dimensional breakdown voltage model of SOI RESURF lateral power device based on lateral linearly graded approximation

Zhang Jun, Guo Yu-Feng, Xu Yue, Lin Hong, Yang Hui, Hong Yang, Yao Jia-Fei
Chin. Phys. B . 2015, 24(2): 028502. **doi:** 10.1088/1674-1056/24/2/028502

An analytical model for the vertical electric field distribution and optimization of high voltage REBULF LDMOS

Hu Xia-Rong, Lü Rui
Chin. Phys. B . 2014, 23(12): 128501. **doi:** 10.1088/1674-1056/23/12/128501

Low on-resistance high-voltage lateral double-diffused metal oxide semiconductor with a buried improved super-junction layer

Wu Wei, Zhang Bo, Luo Xiao-Rong, Fang Jian, Li Zhao-Ji
Chin. Phys. B . 2014, 23(3): 038503. **doi:** 10.1088/1674-1056/23/3/038503

A snapback-free TOL-RC-LIGBT with vertical P-collector and N-buffer design*

Weizhong Chen(陈伟中)[1,2,†], Yao Huang(黄垚)[1,‡], Lijun He(贺利军)[1], Zhengsheng Han(韩郑生)[2,3], and Yi Huang(黄义)[1]

[1] College of Electronics Engineering, Chongqing University of Posts and Telecommunications, Chongqing 400065, China

[2] Institute of Microelectronics, Chinese Academy of Sciences, Beijing 100029, China

[3] University of Chinese Academy of Sciences, Beijing 100049, China

(Received 9 April 2018; revised manuscript received 17 May 2018; published online 25 July 2018)

A reverse-conducting lateral insulated-gate bipolar transistor (RC-LIGBT) with a trench oxide layer (TOL), featuring a vertical N-buffer and P-collector is proposed. Firstly, the TOL enhances both of the surface and bulk electric fields of the N-drift region, thus the breakdown voltage (BV) is improved. Secondly, the vertical N-buffer layer increases the voltage drop V_{PN} of the P-collector/N-buffer junction, thus the snapback is suppressed. Thirdly, the P-body and the vertical N-buffer act as the anode and the cathode, respectively, to conduct the reverse current, thus the inner diode is integrated. As shown by the simulation results, the proposed RC-LIGBT exhibits trapezoidal electric field distribution with BV of 342.4 V, which is increased by nearly 340% compared to the conventional RC-LIGBT with triangular electric fields of 100.2 V. Moreover, the snapback is eliminated by the vertical N-buffer layer design, thus the reliability of the device is improved.

Keywords: reverse-conducting lateral insulated-gate bipolar transistor (RC-LIGBT), breakdown voltage, snapback phenomenon

PACS: 85.30.De, 85.30.Pq, 85.30.Tv **DOI:** 10.1088/1674-1056/27/8/088501

1. Introduction

Lateral insulated gate bipolar transistor (LIGBT) is widely applied to power integrated circuits (ICs) due to its voltage control and low power dissipation.[1–3] On the one hand, the breakdown voltage (BV) is a key property for the LIGBT and it is improved by the trench oxide layer (TOL) technology.[4–6] On the other hand, the reverse conduction capability is another key property for the LIGBT, and the reverse conducting LIGBT (RC-LIGBT) is introduced to integrate the IGBT and the free-wheeling diode (FWD) into one monolithic chip.[7,8] However, the snapback problem is observed due to the short effects of the N-collector at the forward conduction state.[9–12] In recent years, several advanced structures have been proposed to solve this issue.[13–18] The snapback mechanisms and models were given by the voltage drop V_{PN} of the P-collector/N-buffer junction.[19,20] The V_{PN} model is an effective way to suppress the snapback by increasing the doping of the N-drift, but the breakdown voltage will be decreased due to the electric field. On the other hand, the snapback can be suppressed by increasing the resistance of the lateral N-buffer layer. However, it also has adverse influence on the breakdown voltage because the N-buffer acts as the electric field stop layer. Therefore, increasing the breakdown voltage and suppressing the snapback contradict each other.

In this paper, a novel RC-LIGBT with TOL inserted in the N-drift and a vertical N-buffer layer sandwiched between the TOL and P-collector is proposed to improve the breakdown voltage at the reverse breakdown state and eliminate the snapback at the forward conduction state.

2. Device structures and key parameters

Figure 1 shows the structures and key parameters for the devices. Figure 1(a) shows the conventional RC-LIGBT with lateral N-buffer and P-collector in the collector. Figure 1(b) shows the proposed RC-LIGBT with TOL inserted in the N-drift and a vertical N-buffer layer sandwiched between the TOL and the P-collector. A PN junction is formed between the P-collector and the N-buffer for both devices. The two devices are designed with the same parameters except the N-buffer and the P-collector. For both devices, the doping of the N-drift region is 5×10^{14} cm^{-3}, the thickness and the width of the N-drift region are 25 μm and 17 μm, and the thickness of

*Project supported by the National Natural Science Foundation of China (Grant No. 61604027), the Basic and Advanced Technology Research Project of Chongqing Municipality, China (Grant No. cstc2016jcyjA1923), the Scientific and Technological Research Foundation of Chongqing Municipal Education Commission, China (Grant No. KJ1500404), the Youth Natural Science Foundation of Chongqing University of Posts and Telecommunications, China (Grant Nos. A2015-50 and A2015-52), the Chongqing Key Laboratory Improvement Plan, China (Chongqing Key Laboratory of Photo Electronic Information Sensing and Transmitting Technology) (Grant No. cstc2014pt-sy40001), and the University Innovation Team Construction Plan Funding Project of Chongqing, China (Architecture and Core Technologies of Smart Medical System) (Grant No. CXTDG201602009).

†Corresponding author. E-mail: cwz@cqu.edu.cn

‡Corresponding author. E-mail: 632752486@qq.com

© 2018 Chinese Physical Society and IOP Publishing Ltd

the buried oxide (BOX) and the doping of the P-substrate are 2 μm and 8×10^{14} cm^{-3}, respectively. Additionally, the thickness and the width of the TOL are 22 μm and 10 μm for the proposed RC-LIGBT, and the width of the vertical N-buffer W_n and the P-collector W_p can be adjusted. The electric characteristics of the devices are investigated by the MEDICI,[21] and the physical and electrical models such as mobility, ionization, and the recombination models are adopted.

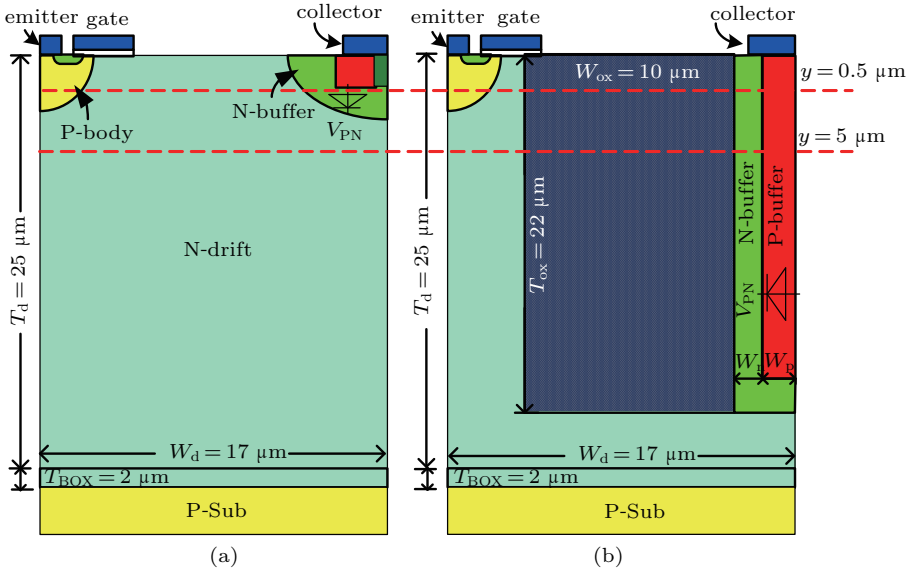


Fig. 1. (color online) Structures and key parameters of (a) conventional RC-LIGBT with lateral N-buffer in the collector, and (b) proposed RC-LIGBT with trench oxide layer and vertical N-buffer in the collector.

3. Results and discussion

3.1. Reverse breakdown voltage BV

At the breakdown state, the gate electrode and the emitter electrode of the device are connected to the ground. $V_{Gate} = 0$ V, $V_{Emitter} = 0$ V, and the collector electrode $V_{Collector}$ is applied with positive voltage. The collector current and the voltage curves are shown in Fig. 2 for the RC-LIGBTs. The doping of the N-drift N_{drift} determines the slope of the electric field, and BV will increases with the decrease of N_{drift}. The simulation shows that when N_{drift} decreases from 1×10^{15} cm^{-3} to 3×10^{14} cm^{-3}, BV increases from 238 V to 342.4 V for the proposed RC-LIGBT, and from 73.7 V to 100.2 V for the conventional RC-LIGBT. Thus the BV of the proposed RC-LIGBT is improved by 340% compared to that of the conventional RC-LIGBT at $N_{drift} = 3 \times 10^{14}$ cm^{-3}. Moreover, device A without TOL and device B with a right vertical N-buffer layer (illustrated in Fig. 3) are also investigated. Device A has the BV of 102 V and device B has the BV of 230 V.

Figure 3 shows the equi-potential contours and the depletion layers of the RC-LIGBTs at breakdown state. For the conventional RC-LIGBT, the equi-potential contours are sparse and laterally distributed at the surface of the N-drift when the device breaks down at the voltage of 100.2 V. The depletion layer is extended to the lateral N-buffer, which indicates that the N-drift is laterally depleted with maximum BV as shown in Fig. 3(a). For the proposed RC-LIGBT, the device will breakdown at the voltage of 342.4 V, and the equi-potential contours are much denser both at the surface and bulk of the N-drift. The depletion layer is extended laterally to the N-buffer and vertically to the BOX as shown in Fig. 3(b). For device A without TOL as shown in Fig. 3(c), the equi-potential contours are almost the same as the conventional RC-LIGBT. For device B as shown in Fig. 3(d) with the right vertical N-buffer layer, the equi-potential contours are sparser than the proposed RC-LIGBT.

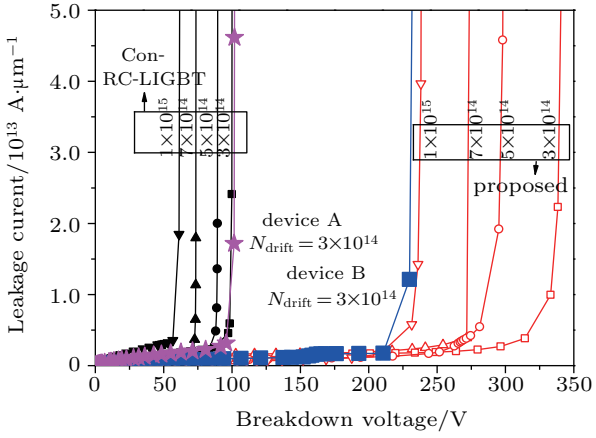


Fig. 2. (color online) Comparison of the breakdown characteristics of the devices as the N-drift doping changes from 1×10^{15} cm^{-3} to 3×10^{14} cm^{-3}. Device A and device B are illustrated in Fig. 3.

Figure 4 provides the surface and bulk electric field distributions for the devices. At the cutline $y = 0.5$ μm as shown in Fig. 4(a), the interface of the surface is formed by SiO_2/Si for the conventional RC-LIGBT and SiO_2/SiO_2 for the proposed. The surface maximum electric field is improved from 2.8×10^5 V/cm for the conventional RC-LIGBT to 6×10^5 V/cm for the proposed RC-LIGBT at the source region, and another peak electric field of 3.2×10^5 V/cm is introduced at the collector region for the proposed RC-LIGBT, thus

it exhibits a trapezoidal electric field distribution. Compared to the conventional RC-LIGBT with triangular electric fields in the N-drift, the breakdown voltage is greatly improved. For device A without TOL, the electric field is also triangular distributed as the conventional RC-LIGBT. For device B, the left and the right peak electric fields are 5.7×10^5 V/cm and 2.2×10^5 V/cm, respectively, which are lower than the proposed RC-LIGBT because the vertical N-buffer is designed to the right and less effective to stop the lateral electric field. At the cutline $y = 5$ μm as shown in Fig. 4(b), the N-drift region is formed by Si/Si for the conventional RC-LIGBT and Si/SiO_2 for the proposed, the bulk electric field is improved from 1×10^5 V/cm for the conventional to 2.6×10^5 V/cm for the proposed. Another peak electric field of 2.4×10^5 V/cm is also introduced at the collector region for the proposed RC-LIGBT, thus the bulk electric field is greatly improved.

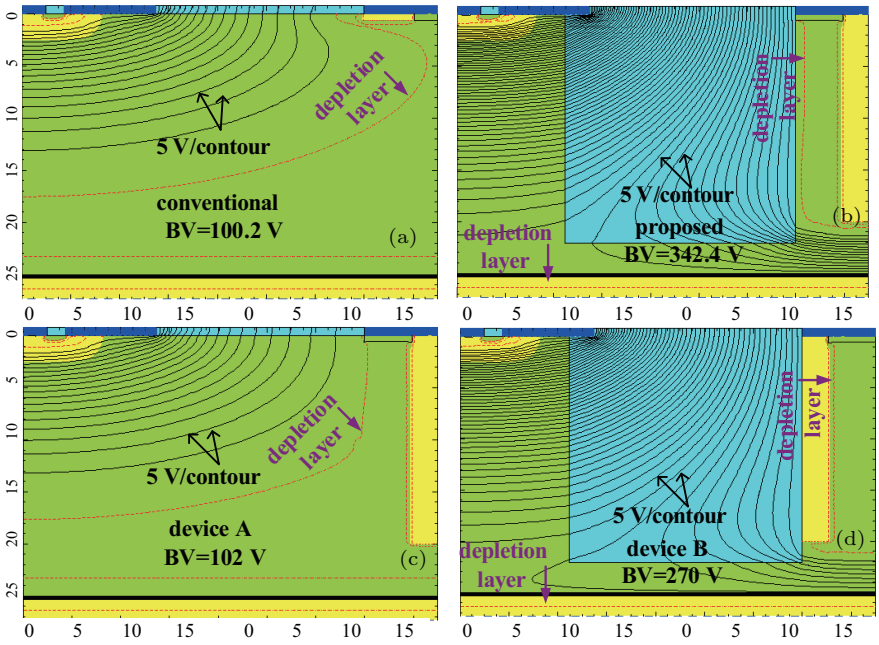


Fig. 3. (color online) Equi-potential contours of (a) the conventional RC-LIGBT, (b) the proposed RC-LIGBT, (c) device A without TOL, and (d) device B with right vertical N-buffer layer.

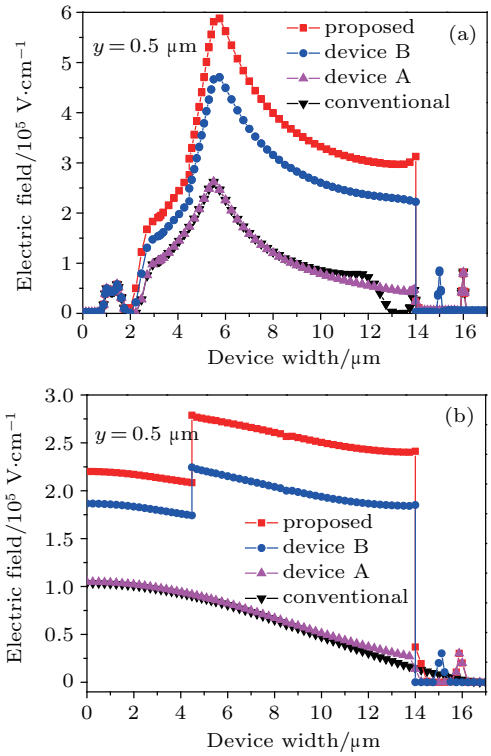


Fig. 4. (color online) The electric field distributions for the conventional RC-LIGBT, proposed RC-LIGBT, device A, and device B. (a) Surface field at the cutline $y = 0.5$ μm (illustrated in Fig. 1), and (b) Bulk field at the cutline $y = 5$ μm (illustrated in Fig. 1).

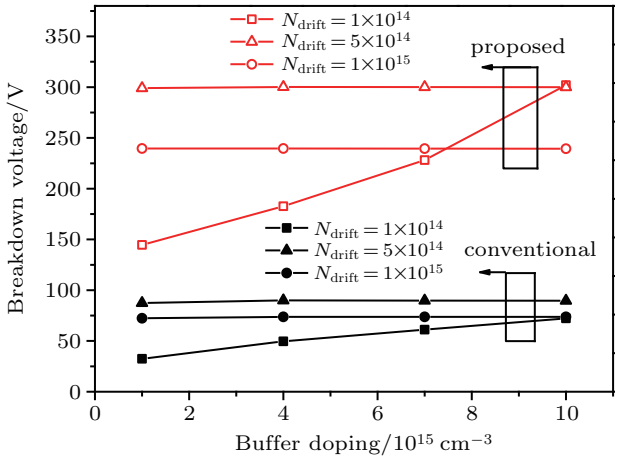


Fig. 5. (color online) The breakdown voltage BV as a function of the N-drift and N-buffer doping for the RC-LIGBTs.

Figure 5 shows the BV as a function of the doping of the N-drift and N-buffer. At the $N_{drift} = 1 \times 10^{14}$ cm^{-3}, the BV of the proposed RC-LIGBT increases significantly with the increase of the N-buffer. However, it will remain constant at $N_{drift} = 5 \times 10^{14}$ cm^{-3} and $N_{drift} = 1 \times 10^{15}$ cm^{-3}. More importantly, at the same value of the N_{buffer}, the BV will increase when the N_{drift} changes from 1×10^{14} cm^{-3} to 5×10^{14} cm^{-3}, but it will decrease when the N_{drift} increases

from 5×10^{14} cm^{-3} to 1×10^{15} cm^{-3}, and the maximum BV is obtained when the N_{drift} is 5×10^{14} cm^{-3}. This phenomenon is also observed for the conventional RC-LIGBT, i.e., the breakdown voltage has a maximum value when the N_{drift} is 5×10^{14} cm^{-3}.

3.2. Snapback Characteristics

At the forward conduction state, the emitter electrode of the device is connected to the ground $V_{\text{Emitter}} = 0$ V. The gate electrode is added with $V_{\text{Gate}} = 15$ V, and positive voltage is applied to the collector electrode as $V_{\text{Collector}}$. The collector current and the voltage curves are shown in Fig. 6. For the conventional RC-LIGBT, with the increase of the $V_{\text{Collector}}$, the conduction mode changes from unipolar mode (conducts with electron at point A) to bipolar mode (conducts with electron and hole at point B) due to the short effects of the N-collector. The inner mechanisms of the snapback are given by the inset picture of Fig. 6. From point O to point A, the electron current is injected from the N^+ emitter and it flows laterally through the N-drift to the lateral N-buffer, and finally to the N-collector. The voltage drop V_{PN} for the P-collector/N-buffer junction is lower than 0.7 V at the moment. From point A to point B, the V_{PN} reaches 0.7 V and the P-collector starts to inject holes to the N-drift, thus the current increases abruptly and then the snapback occurs. For the proposed RC-LIGBT, the N-buffer is vertically designed and the length of the electron channel is much longer than that of the lateral N-buffer, thus the V_{PN} can easily reach 0.7 V and the P-collector can inject holes at the collector voltage $V_{\text{Collector}} = 1.2$ V when $N_{\text{drift}} = 5 \times 10^{14}$ cm^{-3}. Moreover, the snapback is completely eliminated when $N_{\text{drift}} = 1 \times 10^{15}$ cm^{-3}.

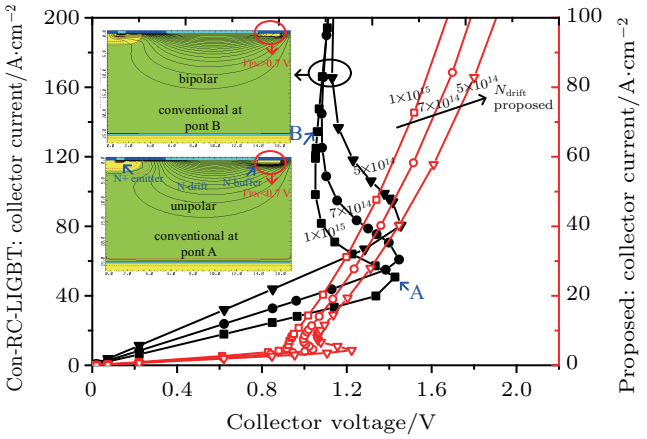


Fig. 6. (color online) Forward conduction characteristics of the conventional and the proposed RC-LIGBT, the inset pictures are for the conventional RC-LIGBT at point A and point B.

Figure 7 shows the influence of the N-buffer doping on the snapback characteristic of the RC-LIGBTs. For the conventional RC-LIGBT, when the electron current flows through the N-buffer, the voltage drop V_{PN} is introduced. However, it is hard to reach 0.7 V because the N-buffer is laterally designed, as illustrated in the inset picture of Fig. 7. When the doping of the N-buffer decreases from 1×10^{16} cm^{-3} to 5×10^{15} cm^{-3}, the snapback can be suppressed, but cannot be eliminated. For the proposed RC-LIGBT, the V_{PN} is much higher than that of the conventional because the N-buffer is vertically designed, and the snapback can be eliminated when N_{buffer} is 5×10^{15} cm^{-3}.

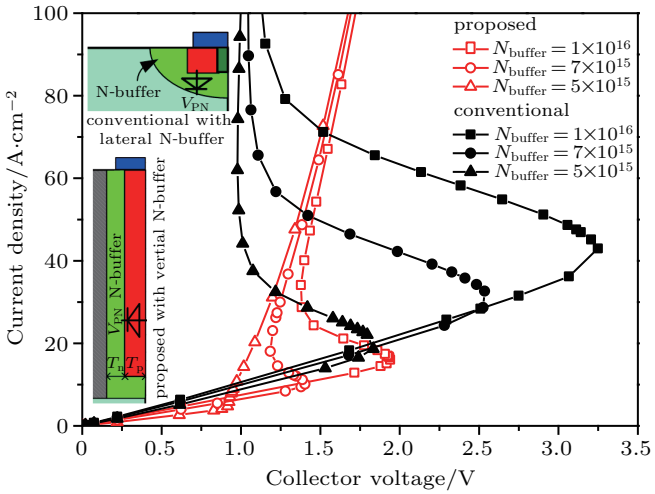


Fig. 7. (color online) The influence of the doping of the N-buffer on the forward conduction characteristic of the RC-LIGBTs; the inset pictures are the conventional RC-LIGBT with lateral N-buffer and the proposed RC-LIGBT with vertical N-buffer.

3.3. Reverse conduction characteristics

At the reverse conduction state, the emitter electrode V_{Emitter} of the device is connected to the positive voltage. The gate electrode and the collector electrode are connected to the ground, i.e., $V_{\text{Gate}} = 0$ V and $V_{\text{Collector}} = 0$ V. The devices are working at the diode mode, with the P-body acting as the anode and the N-collector acting as the cathode of the diode. Figure 8 shows the influence of the doping N_{buffer} on the reverse conduction of the RC-LIGBTs. For the proposed RC-LIGBT, the N-buffer is vertically designed and acts as the electron current channel, thus the reverse conduction capability will be improved when the N_{buffer} increases from 5×10^{15} cm^{-3} to 1×10^{16} cm^{-3}. However, the reverse voltage drop is 1.78 V at 100 A/cm^2 when the $N_{\text{buffer}} = 1\times10^{16}$ cm^{-3}, which is higher than that of the conventional RC-LIGBT with 0.85 V.

W_{n} and W_{p} are the widths of N-buffer and P-collector, respectively, as illustrated in Fig. 1. Figure 9 shows the influence of the ratio $W_{\text{n}}/W_{\text{p}}$ on the reverse conduction of the RC-LIGBTs. For the proposed RC-LIGBT, the width W_{n} of the electron current channel will be improved with the increase of the ratio $W_{\text{n}}/W_{\text{p}}$, as shown in the inset picture, so the reverse conduction capability will be improved when the ratio $W_{\text{n}}/W_{\text{p}}$ changes from 1:2 to 3:1. The reverse voltage drop is 1.58 V at 100 A/cm^2 when the ratio $W_{\text{n}}/W_{\text{p}} = 3:1$.

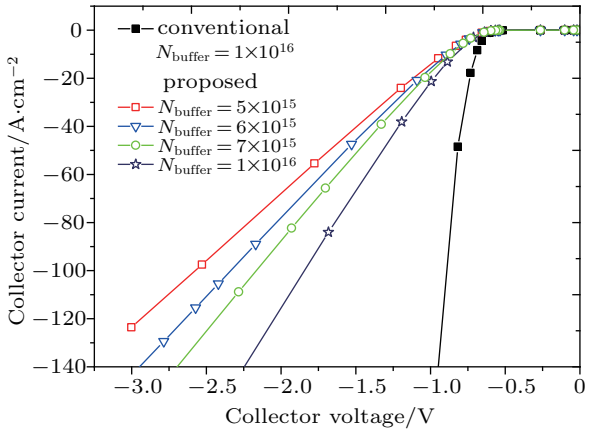


Fig. 8. (color online) The influence of the doping N_{buffer} on the reverse conduction for the RC-LIGBTs.

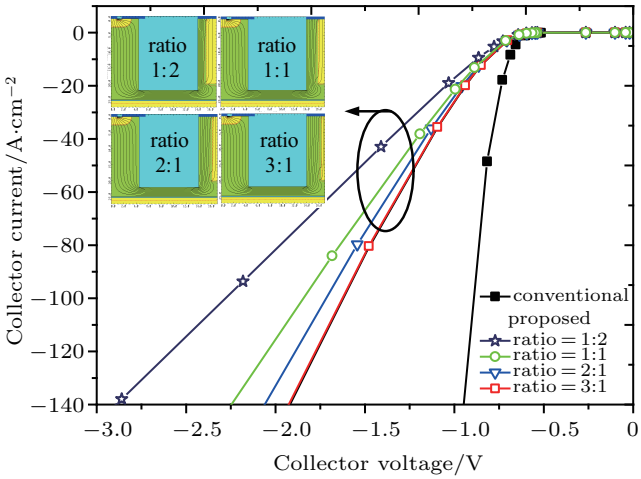


Fig. 9. (color online) The influence of the ratio W_n/W_p on the reverse conduction for the RC-LIGBT; the inset pictures are the current distribution for the proposed RC-LGBT.

3.4. Turn-off characteristics

The switching test circuit shown in Fig. 10 is used to investigate the turn-off performance.[13] In the simulation, the diode is idea, the gate resistor R_g is 10 Ω, the stray inductance L_s is 10 μH, the gate voltage V_g changes from 20 V to −5 V, with a frequency of 5 kHz and a 50% duty cycle to control the device's turning on and off. In addition, the bus voltage is set as 200 V for the proposed RC-LIGBT, and 60 V for the conventional LIGBT (the V_{bus} is set as 60% of the breakdown voltage).

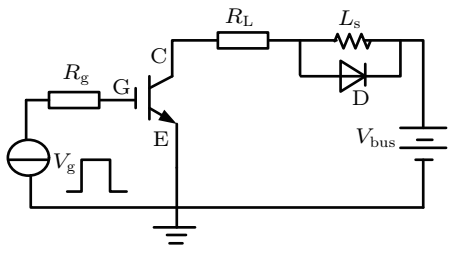


Fig. 10. The resistance load switching test circuit with $R_g = 10$ Ω, $L_s = 10$ μH, and $V_{bus} = 200$ V for the proposed RC-LIGBT, $V_{bus} = 60$ V for the conventional LIGBT (V_{bus} is set as the 60% of BV of the devices).

The switching current and voltage waveforms are shown in Fig. 11. The devices are turned off at the same current density 100 A/cm^2. The turn-off time T_{off} is calculated from 90% IC to 10% IC. For the proposed structure, the vertical N-buffer acts as the fast path for extracting the excess carriers in the N-drift, as the results show the T_{off} are 980 ns and 630 ns for the proposed device with $T_{ox} = 22$ μm and $T_{ox} = 11$ μm. The T_{off} is 310 ns for the conventional RC-LIGBT (T_{ox} =0). For the conventional LIGBT, the excess carriers disappear only depending on the recombination. The T_{off} is 1.85 μs at the doping $N_{P-Collector} = 8\times10^{17}$ cm^{-3}, and it can be further optimized by the $N_{P-Collector}$. The T_{off} is 1.23 μs and 850 ns for the $N_{P-Collector} = 5\times10^{17}$ cm^{-3} and 3×10^{17} cm^{-3}, respectively.

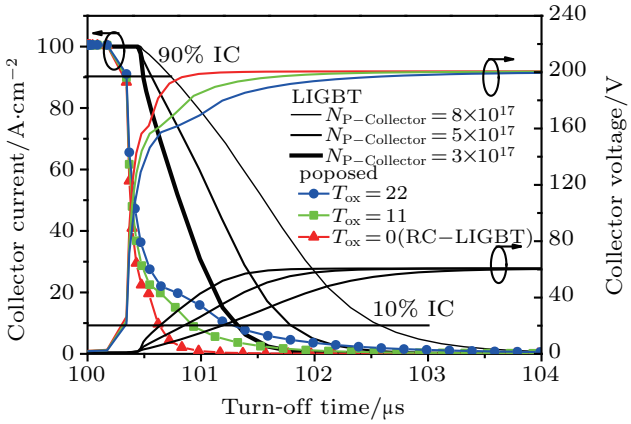


Fig. 11. (color online) Turn-off current and voltage waveforms of the devices under a resistive load switching circuit. $J_F = 100$ A/cm^2, $R_g = 10$ Ω, $L = 10$ μH, and the V_{bus} is set as the 60% of BV of the devices.

Figure 12 shows the influence of the ratio W_n/W_p on the switching property of the proposed RC-LIGBT with $T_{ox} = 22$ μm. The turn-off capability will be improved when the ratio increases from 1:2 to 3:1, and the turn-off time will be reduced from 980 ns to 610 ns due to the enhanced extracting capability of the vertical N-buffer.

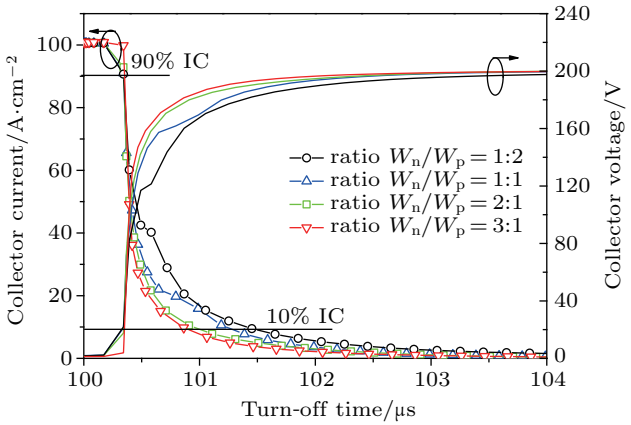


Fig. 12. (color online) The influence of the ratio W_n/W_p on the switching property for the proposed RC-LIGBT with $T_{ox} = 22$ μm.

4. Conclusions

A novel RC-LIGBT with vertical N-buffer and P-collector is proposed. The results show that at the reverse

breakdown state, the BV is greatly improved by 340% with the improvement of the surface and bulk electric field in the N-drift region. Moreover, at the forward conduction state, the snapback can be eliminated by increasing the resistance of the vertical N-buffer. However, at the reverse conduction state, the voltage drop is higher than that of the conventional RC-LIGBT, and can be further optimized by increasing the doping of the N-drift, N-buffer, and the ratio W_n/W_p. Additionally, the turn-off property of the proposed RC-LIGBT is superior to the conventional LIGBT, and it can be optimized by the thickness T_{ox} of the trench oxide and the ratio of W_n/W_p.

References

[1] Zhu J, Zhang L, Sun W, Du Y C, Huang K Q, Chen M, Shi L X, Gu Y and Zhang S 2016 *IEEE Trans. Electron. Dev.* **63** 1161

[2] Sun W, Zhu J, Zhang L, Yu H, D Y C, Huang K Q, Lu S L, Shi L X and Yi Y B 2015 *IEEE Electron. Dev. Lett.* **36** 693

[3] Zhu J, Sun W, Dai W, Zhang L, Liu S L, Shi L X, Yi Y B, Zhang S and Sun W 2014 *IEEE Trans. Electron. Dev.* **61** 3814

[4] Son W S, Sohn Y H and Choi S 2004 *Microelectron. J.* **35** 393

[5] Varadarajan K R, Chow T P, Wang J, Liu R and Gonzalez F 2007 *IEEE ISPSD* **2007** p. 233

[6] Luo X R, Wang Q, Yao G L, Wang Y G and Zhou K 2013 *Chin. Phys. B* **22** 027303

[7] Napoli E, Spirito P, Strollo A G M, Frisina F, Fragapane L and Fagone D 2002 *IEEE Electron Dev. Lett.* **23** 532

[8] Zhang L, Zhu J, Sun W, Du Y C, Yu H, Hua K Q and Shi L X 2015 *IEEE ISPSD* p. 49

[9] Chen W Z, Li Z H, Ren M, Zhang J P, Zhang B, Liu Y, Hua Q, Mao K and Li Z J 2013 *IEEE ISPSD* p. 265

[10] Chen W Z, Li Z H, Zhang B, Ren M, Zhang J P, Liu Y and Li Z J 2014 *Chin. Phys. B* **23** 018505

[11] Byeon D S, Chun J H, Lee B H, Kim D Y, Han M K and Choi Y I 1999 *Microelectron. J.* **30** 571

[12] Chul J H, Byeon D S, Oh J K, Han M K and Choi Y K 2000 *IEEE ISPSD* p. 149

[13] Chen W, Zhang B and Li Z J 2010 *IEEE Electron Dev. Lett.* **31** 467

[14] Zhu J, Zhang L, Sun W, Chen M, Zhou M, Zhao M, Shi L X, Gu Y and Zhang S 2016 *IEEE Trans. Electron Dev.* **63** 2003

[15] Zhu J, Zhang L, Sun W, Chen M, Zhao M, Huang X, Chen J and Qian Y 2017 *IEEE Electron Dev. Lett.* **64** 1187

[16] Sin J K O and Mukherjee S 1991 *IEEE Electron Dev. Lett.* **12** 45

[17] Green D W, Sweet M, Vershinin K V, Hardikar S and Narayanan E M S 2005 *IEEE Trans. Electron Dev.* **52** 2482

[18] Jiang H P, Zhang B, Chen W J, Li Z J, Liu C, Rao Z G and Dong B 2012 *IEEE Electron. Dev. Lett.* **33** 417

[19] Vemulapati U, Kaminski N, Silber D, Storasta L and Rahimo M 2014 *IET Circuits Device Syst.* **8** 168

[20] Chen W Z, Zhang B, Li Z H, Ren M and Li Z J 2012 *IEEE ICSICT* p. 1

[21] Taurus Medici D A V I N C I User's Guides, Synopsys 2013